International Journal of Biochemistry and Cell Biology 113 (2019) 95–102

Contents lists available at ScienceDirect

International Journal of Biochemistry and Cell Biology

journal homepage: www.elsevier.com/locate/biocel

The role of ATF3 in ZnO nanoparticle-induced genotoxicity and cytotoxicity in bronchial epithelial cells

Saisai Wei[a], Tiezheng Li[a], Renxiang Xie[a], Bingqi Ye[a], Jie Xiang[a], Kangli Liu[a], Zhanghui Chen[b], Xiangwei Gao[a,*]

[a] Institute of Environmental Health, and Sir Run-Run Shaw Hospital, and Institute of Environmental Health, Zhejiang University School of Medicine, Hangzhou, 310058, China
[b] Affiliated Hospital of Guangdong Medical University, Zhanjiang, 524000, China

ARTICLE INFO

Keywords:
ZnO nanoparticle
ATF3
DNA repair
Apoptosis
p53

ABSTRACT

ZnO nanoparticle (ZnO NP) exposure causes oxidative stress in the respiratory system, leading to pulmonary damage. Activating transcription factor 3 (ATF3) participates in a variety of cellular stress responses. However, the role of ATF3 in ZnO NP genotoxicity and cytotoxicity remains to be explored. Here we reported that ZnO NP treatment dramatically induced the expression of ATF3 in human bronchial epithelial (HBE) cells, which was mediated by the nuclear factor erythroid 2-related factor 2 (Nrf2). ATF3 was required for the repair of ZnO NP-induced DNA damage as gamma foci number increased when endogenous ATF3 was silenced. Moreover, ATF3 also contributed to ZnO NP-induced cell apoptosis. Mechanistic study revealed that ATF3 interacted with the p53 protein and upregulated its expression under ZnO NP treatment. Collectively, our findings demonstrated ATF3 as an important regulator of epithelial homeostasis by promoting both DNA repair and the death of damaged cells under ZnO NP-induced genotoxic stress.

1. Introduction

Nanoparticles (NPs) are engineered structures with less than 100 nm in at least one dimension. These materials are increasingly being used for diverse industrial and biomedical applications as well as in consumer products (Nel et al., 2006). Among these NPs, zinc oxide nanoparticles (ZnO NPs) are one of the most important metal oxide nanoparticles, which have raised serious concerns about their safety for human health and the environment (Nel et al., 2009). As airway represents the predominant exposure route for ZnO NPs, it becomes imperative to understand the potential toxic effects of ZnO NPs on the human respiratory system and the underlying molecular mechanisms.

Free radical production has been thought to be one of the primary mechanisms of metal or metal oxide nanoparticle toxicity. The production of reactive oxygen species (ROS) by ZnO NPs damages cellular components including DNA (Brown et al., 2014; Nel et al., 2006). Accumulating *in vitro* studies have demonstrated the genotoxicity induced by ZnO NPs in human cells. For instance, ZnO NP-induced DNA breaks were observed in human lung epithelial cell line BEAS-2B and A549 (Heim et al., 2015; Roszak et al., 2016). Upon DNA damage, cells respond by either damage repair or undergoing apoptosis to prevent the risk of becoming tumorigenic. Therefore, the outcome of ZnO NP genotoxicity relies on the interplay of the physicochemical properties of ZnO NPs and cellular responses (Ng et al., 2011). A few proteins, such as p53, have been reported to participate in ZnO NP-induced DNA damage response (Ng et al., 2011). However, other key factors participating in cellular responses to ZnO NPs remain to be identified.

ATF3, a basic leucine zipper (bZIP) DNA binding protein, is a member of the ATF/cAMP-responsive element binding protein (CREB) transcription factor family and can form homodimers or heterodimers with other bZIP proteins to repress or promote transcription (Wei et al., 2014). Although the basal expression is minimal, ATF3 expression is rapidly induced by a wide range of cellular stresses including oxidative stress and DNA damage (Chen et al., 1996). It has been reported that ATF3 plays an important role in maintaining genome stability and promoting DNA damage response (Wang et al., 2018). Studies have also shown that ATF3 engages in the regulation of cell death under stresses (Bar et al., 2016; Turchi et al., 2008). Moreover, ATF3 is positively involved in particulate matter-induced airway inflammation *in vitro* and *in vivo* (Yan et al., 2018). Intriguingly, a recent RNA sequencing study has identified the induction of ATF3 by ZnO NPs, strongly suggesting the involvement of this protein in ZnO NP response (Moos et al., 2011). However, the precise role of ATF3 in ZnO NP toxicity needs to be determined.

* Corresponding author at: Institute of Environmental Medicine, Zhejiang University School of Medicine, 866 Yuhangtang Road, Hangzhou 310058, China.
E-mail address: xiangweigao@zju.edu.cn (X. Gao).

https://doi.org/10.1016/j.biocel.2019.06.007
Received 11 January 2019; Received in revised form 6 May 2019; Accepted 14 June 2019
Available online 17 June 2019
1357-2725/

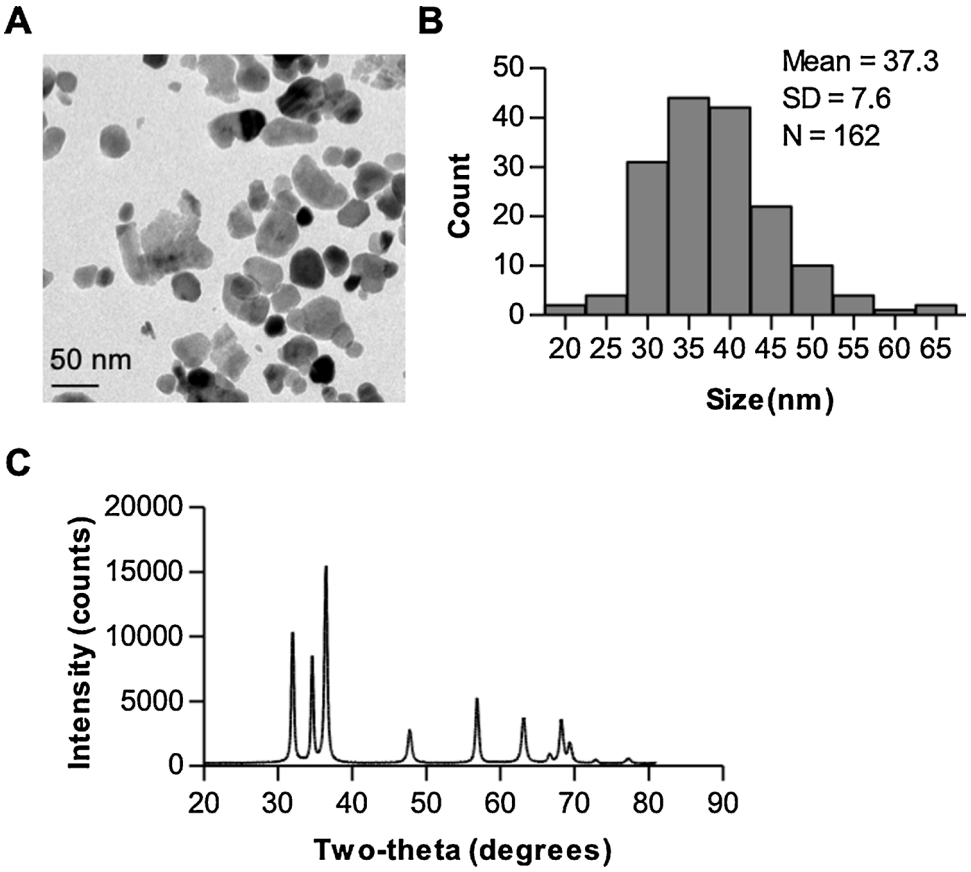

Fig. 1. Characterization of ZnO nanoparticles. (A) Transmission electron microscopy image of ZnO NPs. (B) The size distribution of ZnO NPs. ZnO NPs exhibited good monodispersity and showed approximately normal distribution. (C) XRD analysis of ZnO NPs.

Table 1
Physical characterization of ZnO NPs.

Dispersant	Hydrodynamic size (nm)	Zeta potential (mV)
DMEM + 10% FBS	152.8 ± 6.4	−25.4 ± 0.9
ddH_2O	210.6 ± 5.8	+26.3 ± 1.5

In this study, we evaluated the expression of ATF3 in ZnO NP treatment and the regulatory pathway. Furthermore, we demonstrated an essential role of ATF3 in regulating the genotoxic and cytotoxic effects of ZnO NPs.

2. Materials and methods

2.1. ZnO nanoparticles

ZnO nanoparticle was from Sigma-Aldrich (#637238, Sigma-Aldrich, St. Louis, MO, United States). Nanoparticles were sonicated at 200 W for 30 s prior to cells.

Transmission electron microscope (TEM) was taken by a JEOL JEM-1200EX transmission electron microscope for nanoparticles. ZnO NPs were dispersed in Dulbecco's Modified Eagle Medium (DMEM, Invitrogen, Carlsbad, CA, United States) for 0 h and 24 h and then subjected to dynamic light scattering (DLS) and zeta-potential measurements using the instrument Zetasizer Nano ZS-90 (Malvern Instruments, Orsay, France). X-ray diffraction (XRD) was performed using Bruker D8 Advance diffractometer (Bruker, Billerica, MA, United States) and using CuKα (λ = 1.54 Å) as a radiation source.

2.2. Cells culture and nanoparticle treatment

HBE cells were obtained from ATCC and cultured in DMEM medium supplemented with 10% fetal bovine serum (Thermo Fisher Scientific, Waltham, MA, United States). Cells were maintained at 37 °C in an atmosphere containing 5% CO_2 and 95% humidity.

For ZnO NP treatment, cells were seeded in 6-well or 96-well plates. After 24 h, cells were treated with ZnO NPs suspended in complete DMEM medium at the different concentration for the indicated time and then subjected to further experiments.

2.3. ROS detection

Total ROS was detected by using a fluorescent probe 2′,7′-dichlorofluorescein-diacetate (DCFH-DA) (Sigma-Aldrich). Briefly, cultured HBE cells were treated with or without ZnO NPs for 6 h and then incubated with 10 μM of DCFH-DA at 37 °C for 30 min. After rinsing with PBS to eliminate excess DCFH-DA, cells were harvested in 0.5 ml PBS and the fluorescence intensity was monitored with a flow cytometer (Beckman Coulter, Brea, CA, United States).

2.4. Cell counting Kit-8 (CCK8)-based viability assay

The effect of ZnO NPs on cell viability was assessed by CCK8 assay (Dojindo Laboratory, Japan). HBE cells plated in 96-well plate were transfected with siRNAs for 48 h. Cells were then treated with ZnO NPs for another 24 h. 10 μl of CCK8 reagent was added to each well and the cells were incubated for 2 h at 37 °C. The optical density (OD) at 450 nm was measured by using VarioskanFlash (Thermo Fisher Scientific).

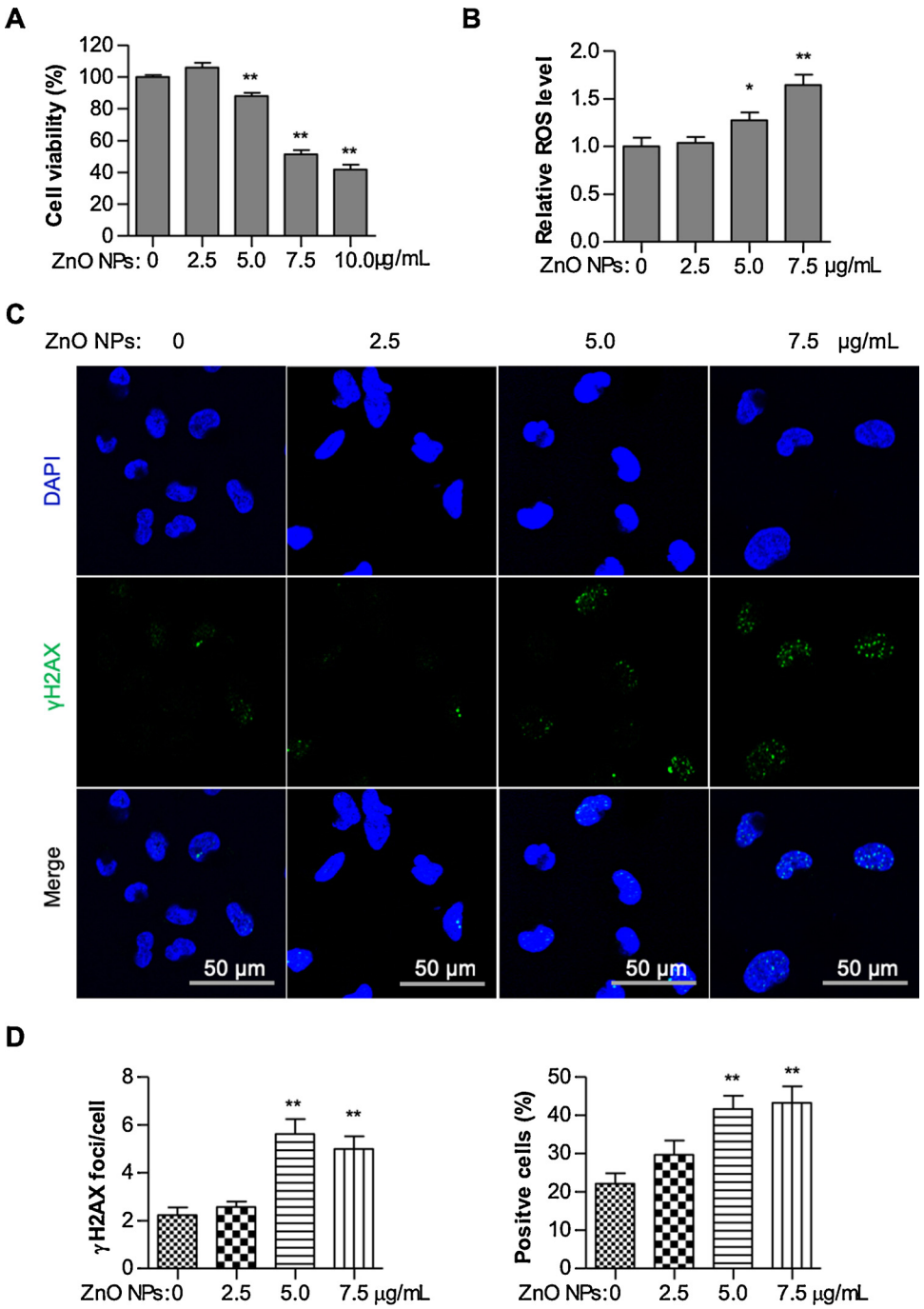

Fig. 2. ZnO NPs induce cytotoxicity and genotoxicity in HBE cells. (A) HBE cells were incubated with ZnO NPs at different concentrations for 24 h and cell viability was determined using CCK-8 assay. (B) HBE cells were incubated with ZnO NPs at different concentrations for 6 h. Intracellular ROS generation was detected by DCFH-DA fluorescent probe and flow cytometry. (C) HBE cells were incubated with ZnO NPs at different concentrations for 6 h and γH2AX foci were detected by immunofluorescence. (D) The average number of γH2AX foci per cell and the percentage of γH2AX foci-positive cells were calculated. All the data are presented as the mean ± SEM of three independent experiments. $^{*}P < 0.05$, $^{**}P < 0.01$ (n = 3, Student's *t*-test).

2.5. 3-(4,5-dimethylthiazol-2-yl)-2,5-diphenyltetrazolium bromide (MTT) assay

MTT assay was performed as described previously (De Vitis et al., 2011; Lombardi et al., 2017). Briefly, cells were plated in 96-well plates with 10^4 cells per well. After overnight incubation, cells were treated with or without ZnO NPs for 24 h. The cell number was determined using a modified MTT assay. The percentage of survival was calculated as the absorbance ratio of treated to untreated cells. The data are presented as the mean ± SEM of 3 independent experiments.

2.6. Apoptosis assay

HBE cells seeded in 6-well plates were transfected with siRNAs for 48 h. After ZnO NP treatment for 12 h, both floating and attached cells were harvested and applied to annexin V detection. Briefly, re-suspended cells were stained with 5 μL of annexin V-FITC (Biovision, Mountain View, CA, United States) for 5 min in the dark and then analyzed by flow cytometry (Beckman Coulter).

2.7. γH2AX immunofluorescence staining

γH2AX staining was performed as described previously (Sun et al., 2018). In brief, after ZnO NP treatment, cells were fixed in 4% paraformaldehyde and then permeabilized in 0.2% Triton X-100 at 4 °C for 15 min. After blocking with goat serum, cells were incubated with γH2AX antibody (Upstate, Temecula, CA, United States) for 2 h at room temperature. After washing, cells were incubated with fluorescein isothiocyanate (FITC)-conjugated goat-anti-mouse secondary antibody (Life Technologies) for 1 h at room temperature. Then, cells were

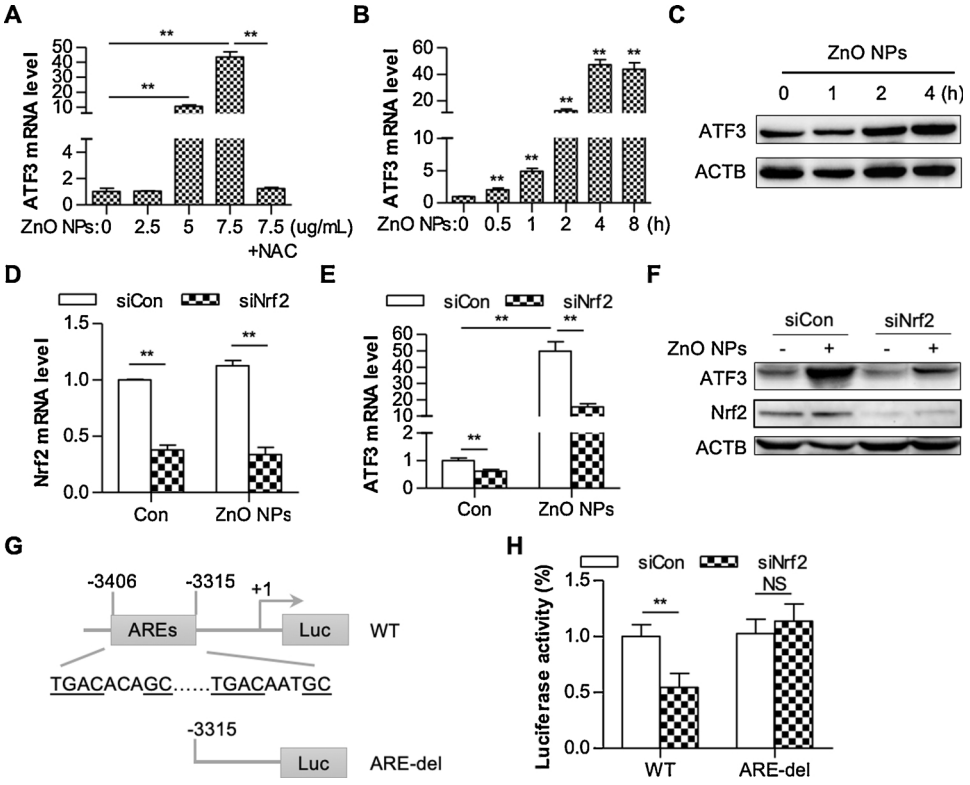

Fig. 3. ZnO NPs stimulate ATF3 transcription through Nrf2 in HBE cells. (A) HBE cells were incubated with ZnO NPs at different concentrations or together with NAC for 8 h. The ATF3 mRNA level was measured by real-time qPCR. (B, C) HBE cells were incubated with 7.5 μg/mL of ZnO NPs and harvested at the indicated time. (B) The ATF3 mRNA level was measured by real-time qPCR. (C) The ATF3 protein level was detected by immunoblotting. (D, E, F) HBE cells transfected with siRNA targeting Nrf2 (siNrf2) or control siRNA were incubated with or without 7.5 μg/mL of ZnO NPs for another 6 h. The mRNA level of Nrf2 (D) and ATF3 (E) was detected by qPCR and the protein level was detected by immunoblotting (F). (G) Schematic of a luciferase reporter of the human ATF3 promoter containing AREs and ARE-deleted promoter. (H) HBE cells transfected with siRNA targeting Nrf2 or control siRNA together with wild-type or ARE-deleted ATF3 promoter luciferase reporter construct. Luciferase activity was measured 24 h following plasmid transfection. The values are the mean ± SEM of three independent experiments. $^{*}P < 0.05$, $^{**}P < 0.01$ (n = 3, Student's *t*-test).

counterstained for 15 min with 4′, 6-diamidino-2-phenylindole (DAPI, Sigma-Aldrich, St. Louis, MO, United States). Finally, a coverslip was mounted for visualization.

The γH2AX foci in the nuclei were photographed using a fluorescent microscope (AX70, Olympus, Tokyo, Japan). The average number of γH2AX foci per cell and the percentage of γH2AX foci positive cells were calculated.

2.8. Plasmids

The plasmid expressing ATF3 was kindly provided by Wen Li (The Second Affiliated Hospital of Zhejiang University School of Medicine). For the construction of ATF3 promoter plasmid, ATF3 promoter or Nrf2-binding site deletion mutant was amplified by PCR and cloned to vector pGL3-basic between *Xho*I and *Hind*III sites. Oligo sequences were listed in Supplemental Table 1.

2.9. RNA purification and reverse transcription reaction

Total RNA was isolated with Trizol reagent (Invitrogen) following the manufacturer's protocol. 0.5 μg of total RNA was reverse transcribed using random hexamers and the High Capacity cDNA Reverse Transcription Kit (Life Technologies, Grand Island, NY, United States).

2.10. Real-time quantitative PCR analysis

Real-time quantitative PCR analysis was performed in 10-μl reactions using SYBR GREEN PCR Master Mix (Applied Biosystems). The related mRNA level was normalized to the *β-actin* mRNA level. Data were analyzed using the $2^{-\Delta\Delta Ct}$method (Livak and Schmittgen, 2001). Sequences of all the primers used for PCR amplification are listed in Supplemental Table 1.

2.11. RNA interference

For knockdown experiments, HBE cells were transiently transfected with 100 pmol of the chemically synthesized siRNAs targeting ATF3 or the negative control siRNA using Lipofectamine2000 (Invitrogen) following the manufacturer's recommendations. Cells were harvested 48 h' post-transfection. siRNAs were synthesized by GenePhama company (Shanghai, China). siRNA sequences used are designed as follows: ATF3 siRNA, forward, GGAGGACUCCAGAAGAUGATT, reverse, UCAU CUUCUGGAGUCCUCCCA; Nrf2 siRNA, forward, GAAUGGUCCUAAAA CACCATT, reverse, UGGUGUUUUAGGACCAUUCTT; negative control siRNA, forward, UUCUCCGAACGUGUCACGUTT, reverse, ACGUGACA CGUUCGGAGAATT.

2.12. Luciferase assay

HBE cells were transfected with ATF3 promoter and pRL-TK as the internal control. 24 h after transfection, cells were treated with ZnO NPs for another 6 h. Cells were then lysed and luciferase activity was measured by the Dual-Luciferase assay system (Promega, Madison, WI, United States). The firefly luciferase activity was normalized to renilla luciferase.

Luciferase-based DNA damage detection was performed as described previously (Turchi et al., 2009). In brief, the pGL3-control plasmid was exposed to high doses of UVC radiation (1000 J/m^2) to induce DNA damage. Damaged and undamaged vectors were then introduced into control or ATF3 knockdown cells. After treatment with 5 μg/mL of ZnO NPs for 6 h, cells were washed and recovered for another 6 h. Cells were then lysed and luciferase activity was measured.

2.13. Co-Immunoprecipitation (Co-IP)

Cells transfected with plasmid expressing FLAG-tagged ATF3 were lysed with RIPA buffer (20 mM Tris-HCl, pH 7.5, 150 mM NaCl, 1 mM EDTA, 1% NP-40) with freshly-added complete protease inhibitor cocktail (Roche Applied Science, Indianapolis, IN). Cell lysates were precipitated with FLAG beads (Sigma) at 4 °C overnight. After washing 3 times with lysis buffer, immunocomplexes were boiled directly in loading buffer and subjected to sodium dodecyl sulfate polyacrylamide

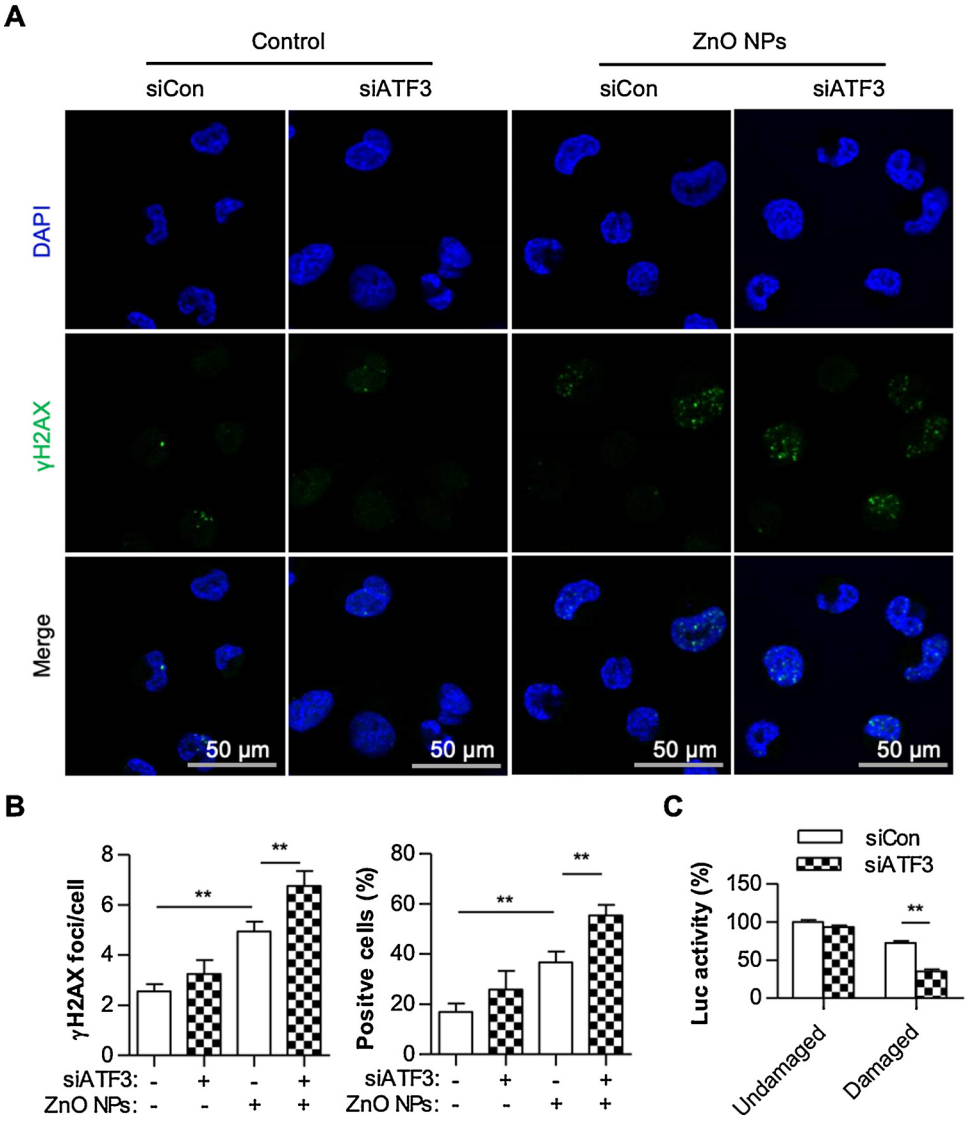

Fig. 4. ATF3 is required for DNA repair during ZnO NP treatment. (A) HBE cells transfected with siATF3 or siCon were treated with or without 5 μg/mL of ZnO NPs for 6 h. γH2AX foci formation was detected by immunofluorescence. (B) The average number of γH2AX foci per cell and the percentage of γH2AX foci-positive cells were calculated. (C) The intact pGL3-control luciferase vectors or the vectors damaged by UVC were transfected into the control cells (siCon) or ATF3 knockdown cells (siATF3). The cells were then exposed to 5 μg/mL of ZnO NPs for 6 h and recovered for another 6 h. The luciferase activity was detected. The values are the mean ± SEM of three independent experiments. $^{**}P < 0.01$ (n = 3, Student's *t*-test).

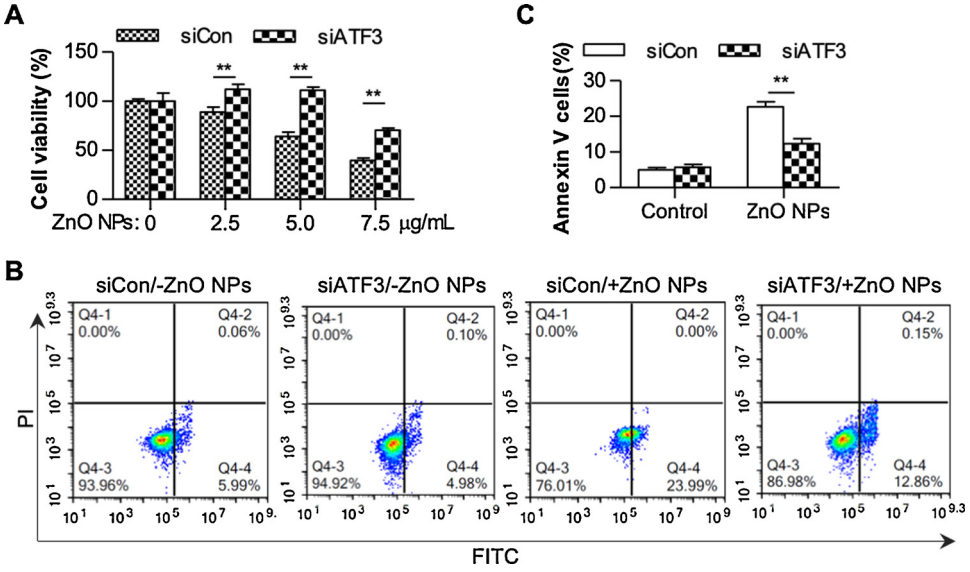

Fig. 5. ATF3 contributes to ZnO NP-induced HBE cell apoptosis. (A, B) HBE cells transfected with siRNA targeting ATF3 (siATF3) or control siRNA (siCon) were treated with or without ZnO NPs at the indicated concentrations for 24 h. (A) Cell viability was determined using cell counting kit-8 (CCK-8). (B) Cell apoptosis was monitored by annexin V-FITC staining and flow cytometry analysis. (C) Annexin-V positive cells were quantified. The values are the mean ± SEM of three independent experiments. $^{**}P < 0.01$ (n = 3, Student's *t*-test).

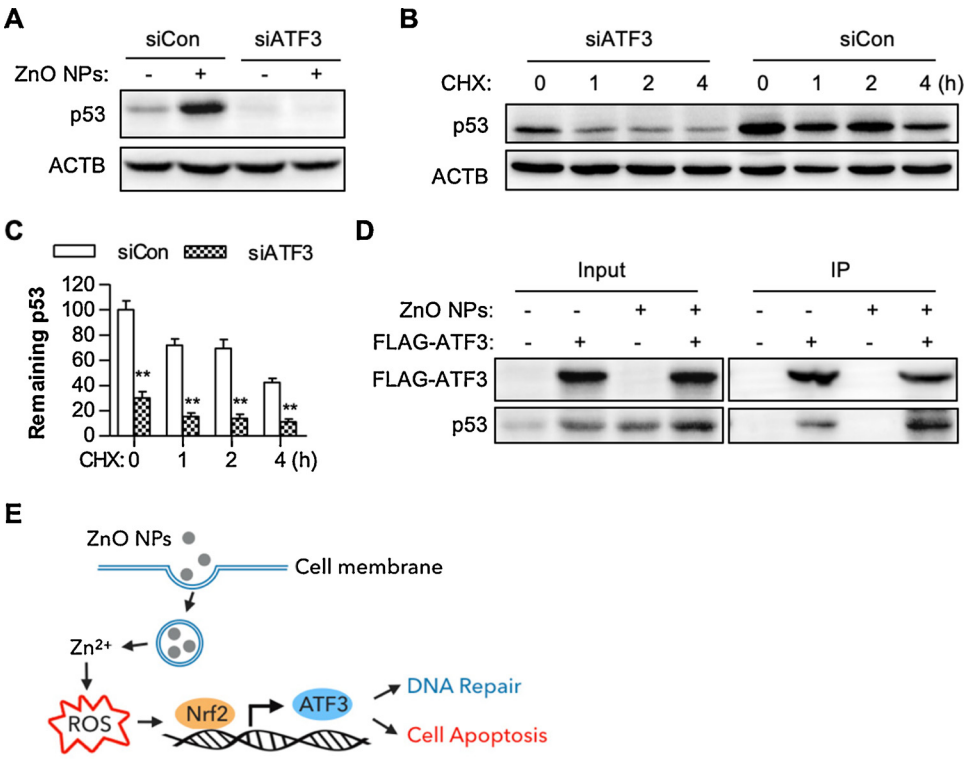

Fig. 6. ATF3 stabilizes the p53 protein. (A) HBE cells transfected with siATF3 or siCon were treated with or without 5 μg/mL of ZnO NPs for 6 h. The protein level of p53 was detected by immunoblotting. (B) HBE cells transfected with siATF3 or siCon were treated with 5 μg/mL of ZnO NPs for 6 h. The protein synthesis was inhibited by CHX and the remaining p53 protein was detected by immunoblotting. (C) The relative p53 intensity in (B) was calculated. (D) HBE cells were transfected with plasmid expressing FLAG-tagged ATF3. Immunoprecipitation was carried out using FLAG antibody and the immunoprecipitated complex was blotted with p53 antibody and ATF3 antibody. (E) Schematic model for the role of ATF3 in ZnO NP-induced DNA damage and cell apoptosis.

gel electrophoresis (SDS-PAGE).

2.14. Immunoblotting analysis

Proteins were quantified by BCA protein assay kit (Bio-Rad) and applied to immunoblotting analysis as described previously (Gao et al., 2014). 50 μg of total proteins were subjected to SDS-PAGE and transferred to nitrocellulose membrane (Whatman, Clifton, NJ, United States). The membrane was blocked with 3% bovine serum albumin (BSA), probed with antibodies targeting to ATF3 (Cell Signaling Technology, Beverly, MA, United States), Nrf2 (Cell Signaling), p53 (Cell Signaling), or ACTB (Cell Signaling). The membrane was incubated with horseradish-conjugated secondary antibodies, detected with the SuperSignal West Pico chemiluminescence substrate (Thermo Fisher Scientific), and finally exposed to an X-ray film.

2.15. Statistical analysis

The experiments were repeated at least three times and data were presented as mean ± SEM. Statistical significance between two groups was determined with the Student's *t*-test. $P < 0.05$ was considered significant.

3. Results

3.1. Characterization of ZnO NPs

Biological responses of the ZnO NPs are highly dependent on their physicochemical properties, including size, shape, and charge (Xu et al., 2010). We therefore first evaluated the size of ZnO NPs using TEM. Data showed that the ZnO NPs we used are pseudo-spherical in shape with the average diameter of 37.3 nm (Fig. 1A). Size measurement by Image J software showed that ZnO NPs were approximately normally distributed (Fig. 1B). ZnO NPs were monodispersed and their hydrodynamic size in full culture media was 152.8 ± 6.4 nm (Table 1). The XRD analysis revealed that the ZnO NPs exhibited a hexagonal structure (Fig. 1C). Further, we measured zeta potentials of ZnO NPs, which provide information on nanomaterials interaction with biomolecules. ZnO NPs were positively charged in water (+26.3 ± 1.5 mV) but negatively charged in full medium (-25.4 ± 0.9 mV, Table 1), indicating the adsorption of the negatively charged serum-derived proteins onto the ZnO NPs.

3.2. ZnO NPs induce cytotoxicity and genotoxicity in HBE cells

Having characterized physicochemical properties of ZnO NPs, we determined the cytotoxicity of ZnO NPs. To this end, both CCK8 and MTT assays were applied. Exposure to 5 μg/mL of ZnO NPs for 24 h significantly reduced cell viability (Fig. 2A, S1). ZnO NPs decreased cell viability in a dose-dependent manner with an estimated LC50 at about 7.5 μg/mL (Fig. 2A). Induction of oxidative stress has been ascribed as the main cause of ZnO NPs toxicity (Nel et al., 2006; Wu et al., 2018). Indeed, we observed that 6 h exposure to 5 μg/mL of ZnO NPs was enough to induce significant elevation of intracellular ROS level in HBE cells (Fig. 2B).

To obtain insights into the possible ZnO NPs genotoxicity, we analyzed DNA-double strand breaks using γH2AX foci staining. We treated HBE cells with ZnO NPs for 6 h because at this time point we did not detect any cell viability loss. Data showed that both the average number of γH2AX foci per cell and the percentage of γH2AX foci positive cells significantly increased in cells treated with ZnO NPs at the concentration of 5 μg/mL, indicating the genotoxic effect of ZnO NPs. 7.5 μg/mL of ZnO NPs did not further increase gamma foci formation (Fig. 2C, D).

3.3. ZnO NPs stimulate ATF3 transcription through Nrf2 in HBE cells

Since ATF3 plays important roles in various stresses, we evaluated the response of ATF3 to ZnO NPs. To this end, we treated HBE cells with ZnO NPs and detected ATF3 expression. ZnO NPs increased ATF3 mRNA level in a dose-dependent manner. ATF3 mRNA level increased to 10.6-fold in cells treated with 5 μg/mL of ZnO NPs for 8 h while increased to 43.6-fold in cells treated with 7.5 μg/mL of ZnO NPs (Fig. 3A). The mRNA level of ATF3 started to increase as early as 0.5 h after ZnO NP treatment, while the protein level started to increase at 2 h

of ZnO NP treatment (Fig. 3B, C). These data indicated that ATF3 is an early responsive gene during ZnO NP treatment.

ROS scavenger NAC almost reduced ATF3 expression to the basal level, implying that the induction of ATF3 relies on ROS signaling (Fig. 3A). Nrf2 is a master transcription factor regulating antioxidant responses (Li et al., 2004; Ma, 2013). To determine the role of Nrf2 in regulating ATF3 expression, endogenous Nrf2 was silenced by siRNA (Fig. 3D, F). Knockdown of Nrf2 resulted in a significant reduction of ATF3 mRNA and protein expression under ZnO NP treatment (Fig. 3E, F), indicating that ATF3 transcription is under the control of Nrf2.

By analyzing the ATF3 gene proximal promoter, we identified two putative antioxidant response elements (AREs), consensus Nrf2-binding sequences (Fig. 3G). To determine the direct regulation of Nrf2 on ATF3 expression, the luciferase reporters containing ATF3 promoters with either wild-type or AREs-deleted sequences were used. Data revealed that luciferase activity of the wild-type ATF3 promoter reporter was significantly reduced (to 50% of control levels) following knockdown of Nrf2. However, deletion of ARE region abolished Nrf2 effect, implying that ATF3 promoter activity is Nrf2-dependent (Fig. 3H).

3.4. ATF3 is required for DNA repair during ZnO NP treatment

Given the induction of ATF3 by ZnO NPs, we investigated the role of ATF3 in ZnO NP-induced genotoxicity. To this end, the expression of ATF3 was down-regulated using siRNA (Fig. S2) and DNA breaks were detected by gamma foci staining. Data showed that the gamma foci significantly increased after ATF3 knockdown (Fig. 4A, B), indicating the augment of DNA damage. To further confirm our results, we quantified the extent of DNA damage by using a luciferase reporter system. Luciferase vector was exposed to UVC to induce DNA damages. Damaged and undamaged vectors were then introduced into control or ATF3 silenced cells. Therefore, the luciferase expression is inversely proportional to the extent of DNA damage. About 72% of luciferase vectors were repaired in control cells whereas only about 35% of luciferase vectors were repaired in ATF3 knockdown cells (Fig. 4C), demonstrating an essential role of ATF3 in DNA repair response during ZnO NP treatment.

3.5. ATF3 contributes to ZnO NP-induced HBE cell apoptosis

Cell apoptosis is one way for the cells to prevent the damaged DNA from being passed down to its progeny. Therefore, we evaluated the function of ATF3 in regulating cell apoptosis during ZnO NP-induced genotoxicity. Both CCK8 and MTT assays showed that the ATF3-deficient cells were resistant to cytotoxic effects of ZnO NPs (Fig. 5A, S3). Annexin V-FITC staining were used for the detection of apoptosis. Data showed that apoptosis was significantly induced after ZnO NP treatment. The apoptotic cells were reduced in the ATF3-silenced cells compared with the control cells, correlating with the attenuated cytotoxicity (Fig. 5B, C). These results demonstrated that ATF3 is essential in mediating cell apoptosis during ZnO NP-induced genotoxicity.

3.6. ATF3 regulates p53 expression

To explore the mechanism of action of ATF3, we first focused on cellular ROS pathway. Knockdown of ATF3 affected neither the expression of Nrf2-target gene HO-1 nor cellular ROS level, implying that ATF3 does not affect Nrf2 signaling (Fig. S4). ATF3 has been reported to interact with p53 protein (Wang et al., 2018; Yan et al., 2005). As p53 is a key factor in regulating DNA repair and apoptosis, we explored the relationship between ATF3 and p53. Data showed that ZnO NP treatment increased p53 protein expression, while knockdown of ATF3 decreased p53 level (Fig. 6A). Using CHX to inhibit protein synthesis, we detected the degradation of p53 protein. Data showed that p53 protein degraded more quickly after ATF3 knockdown (Fig. 6B, C), indicating the destabilization of p53 protein. Co-immunoprecipitation (Co-IP) assay showed that p53 was co-immunoprecipitated by FLAG-ATF3 (Fig. 6D), indicating an interaction between ATF3 and p53. These data suggested that ATF3 binds to p53 and stabilizes p53 protein during ZnO NP treatment.

4. Discussion

The toxicity of ZnO NPs has gained much attention with the fast growth of nanotechnology. Both *in vitro* and *in vivo* evidence has shown that ZnO NPs induce a toxic effect in the respiratory system (Heim et al., 2015; Nel et al., 2006; Roszak et al., 2016; Wu et al., 2018). However, the interplay between ZnO NPs and cellular components is still limited. In this report, we demonstrated ATF3 as an early responsive gene participating in ZnO NP-induced cellular genotoxic stress by playing dual roles. On one hand, ATF3 is required for DNA damage repair and maintenance of genome stability. On the other hand, ATF3 mediates cell apoptosis if the DNA damage is irreparable (Fig. 6E).

The essential role of ATF3 in DNA repair has been consolidated in various conditions. For example, ATF3 is required for the repair of double-strand breaks induced by UV or γ-irradiation (IR) (Turchi et al., 2008). Accordingly, knockdown/knockout of ATF3 expression impairs double-strand break repair and sensitizes cells to irradiation (Cui et al., 2015). Moreover, $Atf3^{-/-}$ mouse embryonic fibroblasts had more aberrant chromosomes and micronuclei and were genetically unstable (Wang et al., 2018). However, the function of ATF3 in cell-fate decisions regarding cell death or survival under these genotoxic conditions remains inconsistent. It was reported that ATF3 could promote UV- and cisplatin-induced cell death (Bar et al., 2016; Turchi et al., 2008). In agreement with these studies, our data revealed that ATF3 is required for cell apoptosis under ZnO NP exposure. However, ATF3 was also reported to protect cells from UV-induced apoptosis by facilitating the recruitment of Tip60 to damaged DNA sites (Cui et al., 2015). These inconsistent results are most probably due to the extent of DNA damage. At a low level of genotoxic stress, ATF3 triggers the DNA repair pathway to restore cellular homeostasis and survival, while at a high level of genotoxic stress, ATF3 mainly induces apoptosis pathway. However, the underlying mechanism remains to be elucidated.

Our data showed that the ROS/Nrf2 signaling mediates the induction of ATF3. First, ROS scavenger NAC almost completely abolished ATF3 induction. Moreover, we identified Nrf2 as a direct transcription factor regulating ATF3 expression, as evidenced by the downregulation of ATF3 in Nrf2 knockdown cells. However, inconsistent with the previous findings that ATF3 contributed to the anti-oxidative and cytoprotective functions of Nrf2 (Brown et al., 2008; Rao et al., 2015), we found that ATF3 has no effect on cellular ROS level and Nrf2-target gene expression in the context of ZnO NP exposure. Instead, ATF3 mainly participates in DNA repair and cell apoptosis through p53, which indicates the complex role of ATF3 during cellular stress responses.

The endogenous p53 is quickly degraded upon MDM2 binding (Haupt et al., 1997), while the protein is stabilized and acts as the central factor in controlling DNA repair and the apoptotic pathways in response to genotoxic stresses (Haupt et al., 1997; Hollstein et al., 1991). Intriguingly, it was reported that ZnO NP exposure results in the activation of p53 and cells lacking p53 are resistant to ZnO NP-induced apoptosis, indicating a role of p53 in ZnO NP toxicity (Ng et al., 2011). Our data indicated ATF3 stabilizes p53 and p53 might acts as the key executor of ATF3 function during ZnO NP treatment. Therefore, the ATF3-p53 might serve as an essential complex guiding the cell fate decision under genotoxic stress induced by ZnO NPs. It should be noted that ATF3 stabilizes and activates the p53 protein in different systems but induces contrast consequences. γ-irradiation-induced apoptosis was significantly suppressed in Atf3 knockout thymocytes and small intestines with impaired p53 activation (Wang et al., 2018). However, ATF3 was also reported to promote p53-mediated DNA repair and suppress cell apoptosis in p53 wild-type cancer cell lines during UV

exposure (Cui et al., 2016). Therefore, the final outcome of the cells exposed to genotoxic stress relies on not only the extent of DNA damage inducer but also the genetic background of the cells.

In summary, we demonstrated that the induction of ATF3 is required for DNA repair and cell apoptosis during ZnO NP treatment. Our results suggested that ZnO NP-induced toxicity is dependent on both nanoparticle properties and the endogenous genetic background of the target cells, such as the expression of key factors including ATF3.

Acknowledgments

This work was supported by grants from National Natural Science Foundation of China (81672847 to X.G.), and Zhejiang Provincial Natural Science Foundation of China (Grant No. LQ19C050004 to S.W., and LY16H040008 to X.S.).

Appendix A. Supplementary data

Supplementary material related to this article can be found, in the online version, at doi:https://doi.org/10.1016/j.biocel.2019.06.007.

References

Bar, J., Hasim, M.S., Baghai, T., Niknejad, N., Perkins, T.J., Stewart, D.J., Sekhon, H.S., Villeneuve, P.J., Dimitroulakos, J., 2016. Induction of activating transcription factor 3 is associated with cisplatin responsiveness in non-small cell lung carcinoma cells. Neoplasia 18 (9), 525–535.

Brown, D.M., Kanase, N., Gaiser, B., Johnston, H., Stone, V., 2014. Inflammation and gene expression in the rat lung after instillation of silica nanoparticles: effect of size, dispersion medium and particle surface charge. Toxicol. Lett. 224 (1), 147–156.

Brown, S.L., Sekhar, K.R., Rachakonda, G., Sasi, S., Freeman, M.L., 2008. Activating transcription factor 3 is a novel repressor of the nuclear factor erythroid-derived 2-related factor 2 (Nrf2)-regulated stress pathway. Cancer Res. 68 (2), 364–368.

Chen, B.P., Wolfgang, C.D., Hai, T., 1996. Analysis of ATF3, a transcription factor induced by physiological stresses and modulated by gadd153/Chop10. Mol. Cell. Biol. 16 (3), 1157–1168.

Cui, H., Guo, M., Xu, D., Ding, Z.C., Zhou, G., Ding, H.F., Zhang, J., Tang, Y., Yan, C., 2015. The stress-responsive gene ATF3 regulates the histone acetyltransferase Tip60. Nat. Commun. 6, 6752.

Cui, H., Li, X., Han, C., Wang, Q.E., Wang, H., Ding, H.F., Zhang, J., Yan, C., 2016. The stress-responsive gene ATF3 mediates dichotomous UV responses by regulating the Tip60 and p53 proteins. J. Biol. Chem. 291 (20), 10847–10857.

De Vitis, S., Sonia Treglia, A., Ulianich, L., Turco, S., Terrazzano, G., Lombardi, A., Miele, C., Garbi, C., Beguinot, F., Di Jeso, B., 2011. Tyr phosphatase-mediated P-ERK inhibition suppresses senescence in EIA + v-raf transformed cells, which, paradoxically, are apoptosis-protected in a MEK-dependent manner. Neoplasia 13 (2), 120–130.

Gao, X., Dong, H., Lin, C., Sheng, J., Zhang, F., Su, J., Xu, Z., 2014. Reduction of AUF1-mediated follistatin mRNA decay during glucose starvation protects cells from apoptosis. Nucleic Acids Res. 42 (16), 10720–10730.

Haupt, Y., Maya, R., Kazaz, A., Oren, M., 1997. Mdm2 promotes the rapid degradation of p53. Nature 387 (6630), 296–299.

Heim, J., Felder, E., Tahir, M.N., Kaltbeitzel, A., Heinrich, U.R., Brochhausen, C., Mailander, V., Tremel, W., Brieger, J., 2015. Genotoxic effects of zinc oxide nanoparticles. Nanoscale 7 (19), 8931–8938.

Hollstein, M., Sidransky, D., Vogelstein, B., Harris, C.C., 1991. p53 mutations in human cancers. Science 253 (5015), 49–53.

Li, N., Alam, J., Venkatesan, M.I., Eiguren-Fernandez, A., Schmitz, D., Di Stefano, E., Slaughter, N., Killeen, E., Wang, X., Huang, A., Wang, M., Miguel, A.H., Cho, A., Sioutas, C., Nel, A.E., 2004. Nrf2 is a key transcription factor that regulates antioxidant defense in macrophages and epithelial cells: protecting against the proinflammatory and oxidizing effects of diesel exhaust chemicals. J. Immunol. 173 (5), 3467–3481.

Livak, K.J., Schmittgen, T.D., 2001. Analysis of relative gene expression data using real-time quantitative PCR and the 2(-Delta Delta C(T)) method. Methods 25 (4), 402–408.

Lombardi, A., Trimarco, B., Iaccarino, G., Santulli, G., 2017. Impaired mitochondrial calcium uptake caused by tacrolimus underlies beta-cell failure. Cell Commun. Signal 15 (1), 47.

Ma, Q., 2013. Role of nrf2 in oxidative stress and toxicity. Annu. Rev. Pharmacol. Toxicol. 53, 401–426.

Moos, P.J., Olszewski, K., Honeggar, M., Cassidy, P., Leachman, S., Woessner, D., Cutler, N.S., Veranth, J.M., 2011. Responses of human cells to ZnO nanoparticles: a gene transcription study. Metallomics 3 (11), 1199–1211.

Nel, A., Xia, T., Madler, L., Li, N., 2006. Toxic potential of materials at the nanolevel. Science 311 (5761), 622–627.

Nel, A.E., Madler, L., Velegol, D., Xia, T., Hoek, E.M., Somasundaran, P., Klaessig, F., Castranova, V., Thompson, M., 2009. Understanding biophysicochemical interactions at the nano-bio interface. Nat. Mater. 8 (7), 543–557.

Ng, K.W., Khoo, S.P., Heng, B.C., Setyawati, M.I., Tan, E.C., Zhao, X., Xiong, S., Fang, W., Leong, D.T., Loo, J.S., 2011. The role of the tumor suppressor p53 pathway in the cellular DNA damage response to zinc oxide nanoparticles. Biomaterials 32 (32), 8218–8225.

Rao, J., Qian, X., Li, G., Pan, X., Zhang, C., Zhang, F., Zhai, Y., Wang, X., Lu, L., 2015. ATF3-mediated NRF2/HO-1 signaling regulates TLR4 innate immune responses in mouse liver ischemia/reperfusion injury. Am. J. Transplant. 15 (1), 76–87.

Roszak, J., Catalan, J., Jarventaus, H., Lindberg, H.K., Suhonen, S., Vippola, M., Stepnik, M., Norppa, H., 2016. Effect of particle size and dispersion status on cytotoxicity and genotoxicity of zinc oxide in human bronchial epithelial cells. Mutat. Res. Genet. Toxicol. Environ. Mutagen. 805, 7–18.

Sun, C., Wei, X., Yimaer, A., Xu, Z., Chen, G., 2018. Ataxia telangiectasia mutated deficiency does not result in genetic susceptibility to 50 Hz magnetic fields exposure in mouse embryonic fibroblasts. Bioelectromagnetics 39 (6), 476–484.

Turchi, L., Aberdam, E., Mazure, N., Pouyssegur, J., Deckert, M., Kitajima, S., Aberdam, D., Virolle, T., 2008. Hif-2alpha mediates UV-induced apoptosis through a novel ATF3-dependent death pathway. Cell Death Differ. 15 (9), 1472–1480.

Turchi, L., Fareh, M., Aberdam, E., Kitajima, S., Simpson, F., Wicking, C., Aberdam, D., Virolle, T., 2009. ATF3 and p15PAF are novel gatekeepers of genomic integrity upon UV stress. Cell Death Differ. 16 (5), 728–737.

Wang, Z., He, Y., Deng, W., Lang, L., Yang, H., Jin, B., Kolhe, R., Ding, H.F., Zhang, J., Hai, T., Yan, C., 2018. Atf3 deficiency promotes genome instability and spontaneous tumorigenesis in mice. Oncogene 37 (1), 18–27.

Wei, S., Wang, H., Lu, C., Malmut, S., Zhang, J., Ren, S., Yu, G., Wang, W., Tang, D.D., Yan, C., 2014. The activating transcription factor 3 protein suppresses the oncogenic function of mutant p53 proteins. J. Biol. Chem. 289 (13), 8947–8959.

Wu, Z., Yang, H., Archana, G., Rakshit, M., Ng, K.W., Tay, C.Y., 2018. Human keratinocytes adapt to ZnO nanoparticles induced toxicity via complex paracrine crosstalk and Nrf2-proteasomal signal transduction. Nanotoxicology 1–15.

Xu, M., Fujita, D., Kajiwara, S., Minowa, T., Li, X., Takemura, T., Iwai, H., Hanagata, N., 2010. Contribution of physicochemical characteristics of nano-oxides to cytotoxicity. Biomaterials 31 (31), 8022–8031.

Yan, C., Lu, D., Hai, T., Boyd, D.D., 2005. Activating transcription factor 3, a stress sensor, activates p53 by blocking its ubiquitination. EMBO J. 24 (13), 2425–2435.

Yan, F., Wu, Y., Liu, H., Shen, H., Li, W., 2018. ATF3 is positively involved in particulate matter-induced airway inflammation in vitro and in vivo. Toxicol. Lett. 287, 113–121.